Second-harmonic imaging of the absolute polar molecular orientation at interfaces

Mathias Flörsheimer,* Maik-Thomas Bootsmann,† and Harald Fuchs
Physical Institute, University of Münster, Wilhelm-Klemm-Straße 10, D-48149 Münster, Germany
(Received 6 July 2001; published 1 March 2002)

Interface specific second-harmonic (SH) and sum-frequency microscopes have been developed recently. In these microscopes, the two-dimensional intensity distribution of the nonlinear signal is used to create an image of the interface structure. In the intensity measurements, however, the phases of the nonlinear signals become obscured. The phases provide information on the *absolute* molecular orientation, which is not accessible in a corresponding linear optical experiment. Here we describe two homodyne techniques for the quantitative measurement of the absolute phases and their two-dimensional distribution. The data can be transformed into the polar molecular orientation field of an interface. As a model example, a Langmuir monolayer of organic molecules, 2-docosylamino-5-nitropyridine, is investigated. The SH and laser light are off resonance with the molecular dipole oscillators. In this case, the electromagnetic theory predicts a signal phase of 90° relative to the laser light. Intensity and homodyne images are taken. Dendritic features are observed in the monolayers. Any local feature which is clearly resolved in the images we consider as an individual sample whose local symmetry and polar order we determine. For the description of the features, it is important to introduce local sample coordinates. As we have shown recently, the point group of the local objects and the axial orientation of their molecules (orientation with an uncertainty of 180°) can be determined from a series of intensity images taken with different polarizer orientations. We may then fix a sample coordinate system at any local feature. One coordinate axis may correspond to the preferential molecular orientation of the feature. Since the absolute orientation of the molecules is not known at this state of the investigations, we may assume an arbitrary polar sign of this coordinate axis as a first hypothesis. If this sign agrees with the real sign of the molecular dipoles, we expect a phase of the SH signal of $+90°$. Since the inversion of a dipole's absolute orientation corresponds with a phase shift of 180° in the SH signal, we expect a phase of $-90°$ if the real dipole orientation is opposite to the local coordinate axis. In the homodyne experiments, the intensity image of the interface is then coherently mixed with a spatially homogeneous SH signal from a reference sample. From the local homodyne intensities and the known phase of the reference signal, the local features' signal phase is calculated. The results ($+90°$, $-90°$) agree with the theory. Thus we can determine the absolute orientation of any local feature. In experiments, carried out near or in resonance, additional phases contribute to the SH signal. We show that the absolute dipole orientation can also be measured in these cases without ambiguity.

DOI: 10.1103/PhysRevB.65.125406 PACS number(s): 78.68.+m, 42.65.−k, 82.45.Mp

I. INTRODUCTION

Optical second-harmonic (SH) and sum-frequency (SF) generation[1] have been developed into versatile surface analytical tools during the last two decades. The techniques take advantage of the fact that second-order nonlinear optical processes are dipole forbidden in centrosymmetric media, but allowed at surfaces and interfaces where the inversion symmetry is necessarily broken. A signal can thus be generated which is specific to the one or few monomolecular layers which form the surface of a centrosymmetric material or the interface between two inversion symmetric media. The techniques can be applied to all kinds of interfaces which are accessible to light including the surfaces of liquids,[1–7] surfaces in vacuum,[8,9] and buried interfaces such as electrode surfaces in electrolytic cells,[1,3,4,6] as well as surfactant layers at liquid/liquid interfaces.[4,7] Also, SH and SF generation have been extensively used to study the silicon/silicondioxide interface[8,9] and semiconductor heterointerfaces[8,9] which are important for the micro- and optoelectronic device technology.

The simplest nonlinear optical experiment is SH generation. Here a spot of an interface is illuminated with high laser light intensities. Usually, the SH signal radiated from the spot is then measured with a photomultiplier. This spatially integrated signal provides information on the symmetry and order of the interface averaged over the area of the spot. Recently, this experiment has been improved in order to provide lateral resolution. Interface-sensitive SH microscopes have been developed by various teams.[10–17] In these experiments, the SH light is used to form an image of the interface structure. In recent imaging studies, we also calibrated the response of our camera using a reference sample with known second-order optical susceptibility.[18] We then showed that the lateral distribution of the SH intensity in the calibrated images can be quantitatively transformed into the corresponding molecular orientation field of the interface.[19]

Recently, also an SF microscope[20] was developed. Here a section of a surface is illuminated with two laser beams. One of the lasers is tunable to the infrared (IR) absorption bands (frequency ω_{IR}) of the sample. The other one provides visible light (frequency ω_{vis}). At the surface, an SF signal (frequency $\omega_{SF}=\omega_{IR}+\omega_{vis}$) is generated which is used for imaging. Tuning the IR laser, the SF intensity from the interface becomes resonance enhanced if the laser frequency is close to a vibrational absorption band of the sample molecules. Thus spectroscopic information[1] on the chemical composition of the interface and on the conformation of the mol-

ecules is obtained. An additional benefit of the SF technique is that the signal appears in the visible spectrum.[1] Its small wavelength as compared with the IR wavelength allows us to take images with high far-field optical resolution. The SF microscope thus represents an interface-specific, chemical-analytical IR microscope with the improved spatial resolution limit of a visible-light microscope.[20]

All microscopes which image the SH and SF intensity distribution of an interface, however, do not take advantage of the full information in the signals because the phase is obscured in the intensity measurement. Similar to linear optics, the phase in a nonlinear optical experiment depends on the spectral distance between the frequency of the probing light and the resonance frequency of the molecular oscillators which are responsible for the signal generation. Reliable phase information is particularly important if the surface signal originates from two (or more) different sources which are out of phase, for example, from the topmost molecules of a substrate and from additional adsorbate species. Then, the total signal can only be understood in terms of magnitudes and phases of all contributions.[14,21]

The phase of the nonlinear signal, however, is additionally useful because it depends on the *absolute* orientation of the molecular dipoles which are responsible for SH and SF generation. The inversion of a dipole's orientation corresponds with a phase shift of 180° in the radiated SH or SF wave. In contrast, the corresponding linear optical signal is independent of the sign of the dipole's orientation. As a result, linear optical experiments such as ellipsometric imaging,[22] Brewster angle microscopy,[23,24] or reflection anisotropy microscopy[25] do not allow one to distinguish between a polar and an axial order of the molecules in a sample. SH and SF experiments are specific to polar order, but from *intensity* measurements alone, the information on the orientation of the dipoles can only be obtained with the uncertainty of 180°. The determination of the absolute polar order requires the additional measurement of the *phases* in the nonlinear signals.

Applying homodyne techniques, the phases can be measured. Such interference experiments have been used in recent spatially integrating SH and SF studies.[14,21,26–38] Here, however, we describe two interface-specific, monolayer-sensitive SH imaging experiments with homodyne detection. The two methods allow the quantitative, two-dimensionally resolved determination of arbitrary phases. The first technique is particularly simple. The second one can be applied more versatile. The paper is organized as follows. In Sec. II, we describe the principle of the experiments. The theory is given in Sec. III. Experimental details are described in Sec. IV. The measurements are presented and interpreted in Sec. V. Then, a discussion of the two homodyne techniques concludes the article.

II. SETUP OF THE MICROSCOPES AND PRINCIPLE OF OPERATION

Figure 1 shows principle schemes of the experiments. Figure 1(a) represents our SH intensity contrast microscope in its simplest version. From this technique, the two homodyne detection experiments [Figs. 1(b) and 1(c)] are derived. In the intensity contrast microscope[12,18] [Fig. 1(a)], a section of a surface is illuminated with a collimated laser beam (frequency ω) applying a transmitted light geometry. Selectively at the surface, an SH signal (frequency 2ω) is generated. It is spectrally separated from the laser radiation. Then, a conventional linear optical polarization microscope uses the harmonic light to create an image of the interface structure on the target of an intensified charge-coupled device (CCD) camera. The interface is observed between polarizers which can be turned azimuthally (not shown in Fig. 1).

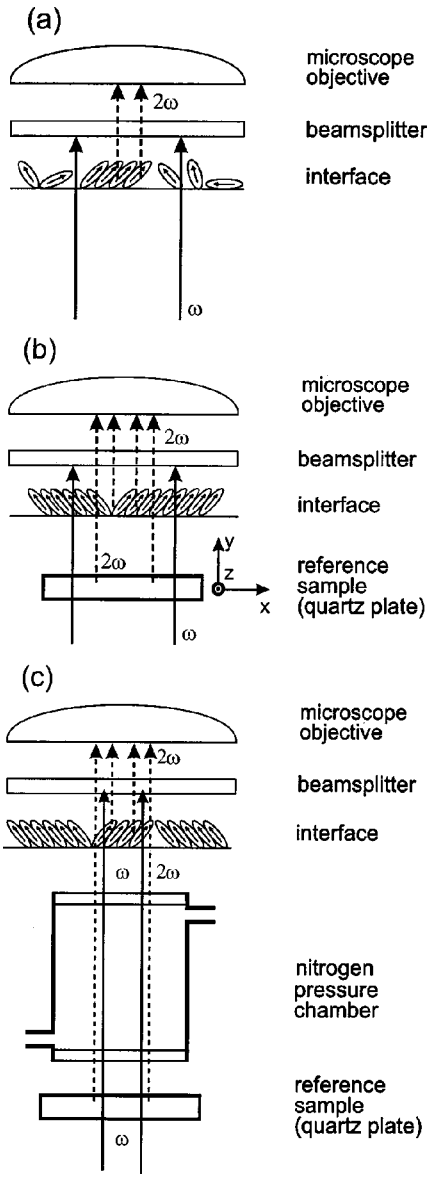

FIG. 1. Principal schemes of the experiments. The fundamental light (frequency ω) and the forward-radiated harmonic signals (2ω) are indicated. The molecules of the interface exhibit dipoles (small arrows). (a) Intensity contrast microscope. (b) Homodyne experiment with a quartz waveplate as reference sample. The quartz crystal can be turned about its *y* axis. (c) Homodyne experiment with an additional pressure cell in order to shift the relative phase of the two harmonic light sources continuously.

The specimen in the experiment may be, for example, the surface of a liquid. In Fig. 1(a), the topmost molecular layer is indicated. In the case shown here, a two-dimensional solid phase coexists with a liquid surface phase. The small arrows represent electric dipoles of the molecules. It can be seen that both phases exhibit a net polar order normal to the surface. The solid phase also exhibits an in-plane polar order. In the experiment of Fig. 1(a), the incident light is polarized in the surface plane. Thus the in-plane polar order is probed here. The normal dipole components can be probed with other experimental geometries[11,12,39] by applying the laser light under oblique incidence.

For simplicity, diffracted SH light which occurs at inhomogeneities of the interface, for example, at the borders of a domain are omitted in Fig. 1. In this article, we consider only direct SH light radiated in forward direction as indicated in Fig. 1. Certainly, direct and diffracted light contributions are required in order to create a sharp image in the microscope. It is important to remember, however, that the light radiated from one object point into the entire acceptance cone of the objective is combined by the microscope near the corresponding image point. The image of a homogeneous object area is mainly composed of direct light. Diffracted SH light contributes mainly to the image of inhomogeneities. The scattered light and its interaction with the nonlinearities of the sample are much more difficult to quantify as compared to the direct light. Thus we use SH imaging here as a quantitative method in the interior of homogeneous areas such as domains at an interface. The technique is not considered as a quantitative tool in a small stripe at the border of a domain whose width corresponds with the resolution of the far-field optical microscope (Abbe's resolution for the SH light).

In the phase-sensitive microscope of Fig. 1(b), a reference sample is additionally introduced into the path of the polarized laser beam. We used a quartz crystal whose bulk is noncentrosymmetric. The reference generates an SH signal with a well-known and stable phase relative to the laser light. The polar axis of the quartz sample is its crystallographic *x* axis [see coordinates in Fig. 1(b)]. The reference can be turned in the plane of the interface (about the *y* axis of the crystal). The thickness of the reference corresponds to a waveplate for the laser light. Thus the polarization state of the fundamental beam is not influenced by the reference.

The SH signal from the quartz crystal and the SH light radiated from the interface in Fig. 1(b) originate from the same laser beam. Thus interference of the SH signals occurs. The interface exhibits a texture with different local features such as dendrites or domains. As an example, two domains are shown schematically at the interface in Fig. 1(b). Their in-plane dipoles are oriented antiparallel to each other. The opposite polar orientation corresponds with a phase difference of 180° in their SH signals. Depending on their orientation relative to the *x* axis of the quartz crystal, one of the domains will appear bright in an image due to constructive interference. Destructive interference will be observed for the other one.

In a recent communication[40] we showed that the qualitative inspection of the images from such a microscope is sufficient to determine the absolute polar orientation of a local feature if its axial orientation (uncertainty of 180°) is already known, for example, from an independent experiment with the intensity contrast microscope of Fig. 1(a). Such investigations, however, do not allow one to determine arbitrary phases quantitatively. To this end, a quantitative measurement and interpretation of the homodyne contrast is required. The quantitative studies will be described below. Also, we use a second phase-sensitive SH microscope [Fig. 1(c)] and compare the results from the two homodyne techniques. In the microscope of Fig. 1(c), the phase difference between the two SH sources can be altered. To this end, a gas cell[31] with variable gas pressure is introduced into the beam path between the reference sample and the interface. A variation of the pressure allows us to alter the refractive index of the gas and its dispersion. Thus the relative phase between the fundamental and the SH reference wave can be changed. This leads to a variation of the phase difference of the SH signals from reference and interface. We will show below that the additional variable microscope parameter allows us to apply this experiment more versatilly as compared with the simpler setup of Fig. 1(b).

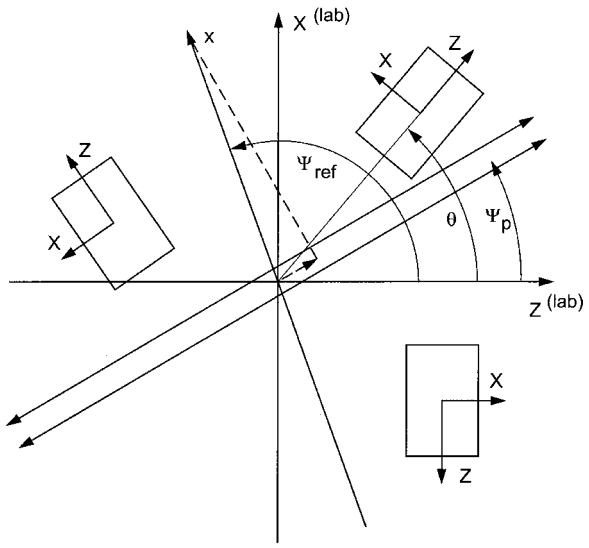

FIG. 2. Experimental geometry in top view onto the interface. An example of a texture with two-dimensional domains is shown. The domains are described with local coordinates (*X*, *Z*). Also, laboratory coordinates ($X^{(\mathrm{lab})}$,$Z^{(\mathrm{lab})}$), the orientations of the polarizers (angle Ψ_{p}), the orientation of the quartz waveplate (angle Ψ_{ref}, polar *x* axis), and the orientation of one of the domains (angle θ) are indicated. The contribution of the signal from the quartz reference to a homodyne image depends on the projection of crystal's *x* axis onto the polarizer orientation (dashed arrow). By turning the reference the amplitude and phase of this projected field can be altered. An inversion of the sign of the projection changes the phase of the reference signal by 180°.

III. THEORY

A. Second-harmonic intensity from the local features of an interface

Figure 2 shows the geometry of the imaging experiments in top view onto the interface. An example of a simple inter-

face texture with various two-dimensional domains is given. Laboratory coordinates $X^{(\mathrm{lab})}$ and $Z^{(\mathrm{lab})}$, which are fixed in the plane of the interface, are indicated. The quartz reference and the polarizers can be arbitrarily turned in the plane. The polar x axis of the quartz crystal makes an angle Ψ_{ref} with respect to the $Z^{(\mathrm{lab})}$ axis. The polarizers are oriented parallel to each other in the experiments of this article. A single angle Ψ_p is thus sufficient to describe their azimuthal position relative to the $Z^{(\mathrm{lab})}$ axis. In order to characterize an individual domain we introduce additional local coordinates X and Z, which are fixed at the crystallographic lattices of the domains. The azimuthal orientation of the local features is described by their angle θ between their local Z axis and the $Z^{(\mathrm{lab})}$ axis. For one of the domains, this angle is indicated in Fig. 2.

We assume that all the domains of the interface exhibit the same crystallographic symmetry and molecular order. Also, the order may be simple in our example. We assume that the dipoles of the SH-active molecular groups may be oriented parallel to the local Z axis. The point group of the domains is then C_S. The property of the domains which describes SH generation is their second-order optical susceptibility tensor $\vec{\vec{d}}$. This quantity can exhibit up to 18 independent elements d_{IJK} where the subscripts J and K refer to the polarization of the incident light fields and I refers to the polarization of the generated SH field. In general, the elements d_{IJK} are complex numbers. If we use local coordinates, the susceptibility tensors for all the domains of the interface are identical because the local features exhibit the same symmetry and order. Additionally, the tensor is particularly simple in our example because we assumed a simple order. Since all the molecular dipoles are parallel to the local Z axis, a single element d_{ZZZ} is sufficient to describe a domain.

In an intensity contrast image (Fig. 2 without quartz reference), the domains of the interface will appear with different brightness because their orientation relative to the polarizers of the SH microscope is different. A domain whose polar axis is oriented favorably ($\theta-\Psi_p=0°$ or $\theta-\Psi_p=180°$) will appear bright. No SH light will be generated for $\theta-\Psi_p=90°$ or $\theta-\Psi_p=270°$. Below, we quantitatively calculate the SH intensity $I^{(2\omega)}$ radiated from the local features of the interface. The intensities in the interference experiment will be considered in Sec. III B.

Various models have been used to describe SH generation at an interface. Applying the model of Mizrahi and Sipe,[41] we obtain

$$I^{(2\omega)}=\frac{2\omega^2L^2}{\varepsilon_0c^3\cos^2\Omega}|d_{\mathrm{eff}}|^2(I^{(\omega)})^2 \tag{1}$$

with $I^{(\omega)}$ the intensity of the fundamental beam, d_{eff} the effective susceptibility, Ω the angle of incidence, L the thickness of the SH-active layer, ε_0 the vacuum permittivity, and c the speed of light in vacuum. In the experiments described here, $\Omega=0°$ (normal incidence). The effective susceptibility depends on the geometry of the experiment (orientation of the polarizers) and on the tensor elements of the sample which contribute to the signal in this geometry. In a coordinate system which is fixed at the polarizers of the experiment, we can express the effective susceptibility of an arbitrary local feature as

$$d_{\mathrm{eff}}=\sum_{UVW}e_U^{(2\omega)}d_{UVW}e_V^{(\omega)}e_W^{(\omega)}, \tag{2}$$

where d_{UVW} represents the tensor elements of the feature and $e_U^{(2\omega)}$, $e_V^{(\omega)}$, and $e_W^{(\omega)}$ are components of polarization unit vectors multiplied by Fresnel factors for the interface.[41] The quantity $e_U^{(2\omega)}$ refers to the polarization of the detected SH field (analyzer orientation); $e_V^{(\omega)}$ and $e_W^{(\omega)}$ refer to the polarization of the incident fields. The susceptibilities in the frame of the polarizers can be obtained from the local susceptibilities d_{IJK} by a coordinate transformation. In our example of an interface, we have

$$d_{\mathrm{eff}}=c_Fd_{ZZZ}\cos^3(\theta-\Psi_p), \tag{3}$$

where the cosine factors account for the projection of the fundamental fields onto the Z axis of the domain and for the projection of the generated SH field from the Z axis onto the analyzer. The quantity c_F represents the product of the Fresnel factors in the experiment.[41] The intensity of a domain in our example is then given by

$$I^{(2\omega)}=\frac{2\omega^2L^2|c_F|^2}{\varepsilon_0c^3}|d_{ZZZ}|^2(I^{(\omega)})^2\cos^6(\theta-\Psi_p). \tag{4}$$

The factor $\cos^6(\theta-\Psi_p)$ describes the dependence of the SH intensity of a local feature on its orientation relative to the polarizers. Also, Eq. (4) shows that the phase of the susceptibility d_{zzz} gets lost when the square of the modulus is calculated or when the SH intensity is measured. The phase can only be obtained from an additional homodyne experiment.

B. Intensities and phases in a homodyne experiment

In a homodyne experiment, the total signal $I_{\mathrm{tot}}^{(2\omega)}$ is given by

$$I_{\mathrm{tot}}^{(2\omega)}=I_{\mathrm{sam}}^{(2\omega)}+I_{\mathrm{ref}}^{(2\omega)}+2\sqrt{I_{\mathrm{sam}}^{(2\omega)}I_{\mathrm{ref}}^{(2\omega)}}\cos\phi, \tag{5}$$

with $I_{\mathrm{sam}}^{(2\omega)}$ and $I_{\mathrm{ref}}^{(2\omega)}$ the SH intensity from the sample and the reference, respectively, and ϕ the phase difference between the harmonic waves. For a homogeneous reference, $I_{\mathrm{ref}}^{(2\omega)}$ is constant for the entire image (if homogeneous illumination is provided). In contrast, $I_{\mathrm{sam}}^{(2\omega)}$ and ϕ, however, may change within the observed area. $I_{\mathrm{sam}}^{(2\omega)}$ can be calculated for the local features of an interface according to Sec. III A. The phase ϕ is composed as

$$\phi=\phi_{\mathrm{sam}}-(\phi_{\mathrm{ref}}+\phi_\Delta), \tag{6}$$

where ϕ_{sam} is the phase of the sample signal which has to be determined in the experiment, ϕ_{ref} is the phase of the reference signal which must be known, and ϕ_Δ is the phase that originates from the distance between the two SH light sources and from the dispersion of the medium between them. For a homogeneous dispersive medium, this phase ϕ_{med} is given by

$$\phi_{\mathrm{med}}=\frac{2L(n^{(\omega)}-n^{(2\omega)})}{\lambda_0}\times 360°, \tag{7}$$

with L the thickness of the medium, $n^{(\omega)}$ and $n^{(2\omega)}$ its refractive indices at the fundamental and harmonic frequency, respectively, and λ_0 the laser wavelength in vacuum. For a material with normal dispersion, ϕ_{med} is negative. A phase shift of 360°, for example, is introduced by a dispersive medium with a thickness of $L_{360}=\lambda_0/2|(n^{(\omega)}-n^{(2\omega)})|$. For air at a laser wavelength of 1064 nm, $L_{360}\approx 13$ cm. The exact value depends on the atmospheric pressure and on other weather parameters. Hence the phase introduced by the air must either be controlled in the homodyne experiment or it must be measured independently.

Since ϕ_{sam} contributes to the argument of a cosine function in Eq. (5), it cannot be determined unambiguously with a single measurement. Hence the experimental conditions must be altered. Two possibilities may be considered. Either ϕ_{ref} or ϕ_Δ can be changed so that various values of cos ϕ are accessible from which ϕ_{sam} may finally be derived. We use both possibilities. In a first series of experiments, we observe an interface with different azimuthal orientations of the quartz reference [experiment of Fig. 1(b)]. Depending on the orientation of the crystal's polar axis relative to the polar axis of a local feature, we can switch between constructive and destructive interference in these experiments. In a second series of measurements, we alter ϕ_Δ by applying the gas pressure cell [experiment of Fig. 1(c)].

C. Reference sample

A benefit of using a bulk specimen as a reference in both types of experiments is the easy handling. The chosen thickness of a waveplate for the fundamental light additionally facilitates the data evaluation. The waveplate does not change the polarization of the laser light. Independent on the orientation of the reference, the interface always experiences the linear polarization state of the fundamental light indicated by the polarizer orientation in Fig. 2. The quartz reference used here is a Y-cut crystal [see coordinates in Fig. 1(b)], which also facilitates the data evaluation. For normal incidence of the laser light as in our experiments, the generation of SH light can easily be described with a single susceptibility[42] tensor element d_{xxx}. The SH light from the reference is thus always polarized parallel to its crystallographic x axis.

Two consequences from the application of a bulk sample as a reference, however, must be considered. The first point is that the SH light which is generated at a certain depth of the quartz crystal suffers a phase shift during its propagation through the material. The phase of the total SH light radiated from the reference in forward direction is given by

$$\phi_{\mathrm{ref}}=\arctan\left(\frac{\sin\frac{4\pi(n^{(\omega)}-n^{(2\omega)})L}{\lambda_0}}{\cos\frac{4\pi(n^{(\omega)}-n^{(2\omega)})L}{\lambda_0}-1}\right), \tag{8}$$

with L the thickness of the plate. It can be seen that L and the refractive indices of the reference sample must be known in order to calculate ϕ_{ref}. Equation (8) can be derived from the coupled wave equations for the nonlinear optical crystal in the nondepleted pump approximation. The calculation and a brief discussion of Eq. (8) follows in the Appendix.

The second consequence from the application of a bulk sample as a reference is that the signal $I_{\mathrm{ref}}^{(2\omega)}$ is usually much larger than the intensity $I_{\mathrm{sam}}^{(2\omega)}$ from an interface or a monolayer if the polar axes of the two SH sources are oriented parallel to each other. In such a case of distinctly different intensities, the introduction of a phase shift of 180° between the interfering signals, either by changing ϕ_{ref} or by changing ϕ_Δ, leads only to a small modulation of the total intensity $I_{\mathrm{tot}}^{(2\omega)}$ [Eq. (5)]. For optimum modulation of the contrast between constructive and destructive interference, however, the intensities from the two sources should be similar. In order to obtain comparable intensities we thus turned the polar axis of the reference crystal with respect to the polarizers.

In Fig. 2, an angle between the reference and the polarizer orientation of $\Psi_{\mathrm{ref}}-\Psi_p=80°$ is shown as an example. In such a case, the intensity from the brightest domains in an experiment might be similar to the intensity from the reference. The local features which generate the highest SH intensity in our example of an interface are those domains whose orientations are either $\theta-\Psi_p=0°$ or $\theta-\Psi_p=180°$. These two groups of domains can readily be distinguished in the homodyne experiment. Constructive interference occurs for one group and destructive interference for the other one. Also, the phase ϕ_{ref} of the reference signal which contributes to the homodyne images can easily be shifted by 180°. To this end, the reference must be turned to angles $\Psi_{\mathrm{ref}}-\Psi_p$ larger than 90°. If the angle of $\Psi_{\mathrm{ref}}-\Psi_p=80°$ in our example is changed to $\Psi_{\mathrm{ref}}-\Psi_p=100°$ contrast inversion will be observed. The determination of the absolute polar orientation and the phases ϕ_{sam} of the local features requires the additional quantitative evaluation of the contrast, which will be given below.

The use of a bulk sample as a reference in a transmitted light geometry as in our homodyne experiments is not optimum if tunable lasers or lasers that provide subpicosecond pulses are desired to be applied in a homodyne microscope. In order to avoid polarization changes in the former case as well as phase distortions and pulse broadening in the latter case such experiments should be carried out with very thin reference samples or with the reference in a reflected light geometry.

D. Expected phase of the sample

We can consider the phase of a local feature at an interface to be composed of two contributions ϕ_{spectr} and ϕ_{SH} according to $\phi_{\mathrm{sam}}=\phi_{\mathrm{spectr}}+\phi_{\mathrm{SH}}$. The phase ϕ_{spectr} is given by the absorption spectrum of the feature and the wavelength of the probing light. The maximum of the longest-wavelength electronic absorption of 2-docosylamino-5-nitropyridine (DCANP) lies at $\lambda=390$ nm. The wavelengths of the fundamental and SH light in our study are consider-

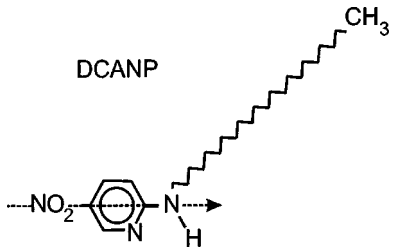

FIG. 3. Structural formula of 2-docosylamino-5-nitropyridine (DCANP) whose monolayers were used as an example. The dipole which corresponds to the predominant optical nonlinearity is indicated.

ably larger. The experiments are thus carried out off resonance with $\phi_{\mathrm{spectr}} \approx 0°$. The phase ϕ_{SH} originates from the SH generation process. Equation (8) describes the phase of an SH signal from a bulk specimen without absorption. For a thin film such as a monolayer, a phase of $\phi_{\mathrm{SH}} \approx 90°$ with respect to the fundamental light is expected (see Fig. 7 in the Appendix). We thus expect a sample phase of $\phi_{\mathrm{sam}} \approx 90°$.

IV. EXPERIMENTAL DETAILS

A Nd:YAG laser (Continuum PL 8000) provided pulses with a wavelength of 1.0642 μm, a duration time of 8 ns, and a repetition rate of 15 Hz. Typical pulse intensities were $\sim$200 MW/cm^2. The detector was a gated-intensified CCD camera (Spectroscopy Instruments ICCD-576 G/RB). Monolayers of DCANP were used as specimens. The structural formula is given in Fig. 3. The permanent molecular dipole which corresponds to the predominant optical nonlinearity of the molecule is also indicated in Fig. 3. In order to acquire an image from a DCANP monolayer, 300 laser pulses were used. Additional details on the intensity imaging experiment are given in Ref. 18.

The waveplate which served as a reference sample was obtained from Steeg & Reuter, Gießen, Germany. It was made of synthetic α-quartz with the refractive index components $n_x^{(\omega)} = 1.534\,13$ and $n_x^{(2\omega)} = 1.546\,90$ at the fundamental and harmonic frequencies, respectively.[43] We controlled the thickness of the waveplate in an additional Maker-fringe experiment[44] to be $L = 2313.0\ \mu\mathrm{m} \pm 0.3\ \mu\mathrm{m}$.

Platelets of fused silica (Hellma, Müllheim, Germany) were used as a substrate for the monolayers. In order to fabricate the films a platelet, cleaned in chromosulfuric acid, was first submerged under Millipore-filtered water. Then, a DCANP monolayer was spread from a mixture of toluene (80 vol %) and decahydronaphthalene onto the water surface. At a lateral pressure of $\sim$1 mN/m and a subphase temperature of $\sim$23 °C, the Langmuir film was finally transferred onto the horizontally oriented substrate by slowly draining off the water. The refractive indices of the substrates were $n^{(\omega)} = 1.449\,68$ and $n^{(2\omega)} = 1.460\,80$.[45] Their thickness was measured in independent experiments. To this end, we cleaned the substrate again. Then, we transferred monolayers of organic dyes[46] onto their front and back sides using the conventional Langmuir Blodgett technique (lifting the vertically oriented substrates). From these samples, Maker fringes were taken which allowed us to calculate the thickness of the platelets to be $L = 1230\ \mu\mathrm{m} \pm 1\ \mu\mathrm{m}$.

In the imaging experiment of Fig. 1(b), it is also important to know the phase shift introduced by the air between the two SH light sources. We calculated this phase from the distance between the two sources and from the length L_{360} for air. The latter quantity we determined at the weather conditions directly after having taken the monolayer images. In this additional experiment, we measured the homodyne signal from two quartz crystals in air as a function of their distance.[31]

For the pressure cell in the other microscopy experiment [Fig. 1(c)], windows of BK 7 glass were used. Their front and back sides were antireflection coated at the fundamental and harmonic frequency (Laser Components, Olching, Germany). In the imaging experiment, the SH light from the quartz waveplate suffers a phase shift when it passes through the windows. Due to the coatings, it is tedious to calculate this shift. We thus carried out an additional set of reference experiments. At first, we took series of homodyne images from a monolayer for various pressures of nitrogen in the gas cell. Then, we replaced the specimen by an additional Y-cut quartz reference (Steeg & Reuter, Gießen) and took another series of homodyne images from the surface of this crystal at various gas pressures. In Sec. V B, the data evaluation will be described. The x axis of the second reference was oriented parallel to the x axis of the waveplate. The second reference was made of natural α-quartz with $n^{(\omega)} = 1.534\,13$ and $n^{(2\omega)} = 1.54702$.[43] Its thickness of $L = 1990.8\ \mu\mathrm{m} \pm 0.3\ \mu\mathrm{m}$ was measured in a Maker-fringe experiment. The absolute polar orientation of the two quartz crystals was determined in two homodyne experiments with a Y-cut $LiNbO_3$ platelet as a reference. The sample with known absolute orientation of its ferroelectric z axis was a gift from N. Kato and Y. Uesu, Waseda University, Tokyo.

V. MEASUREMENTS AND INTERPRETATION

In the homodyne studies described below, we use monolayers of DCANP as a model example because the SH intensity contrast of these films has recently been explained in detail.[18,19,39,47] The films exhibit dendritic structures with irregular macroscopic shapes. On the molecular level, the order, however, is simple. Locally, the in-plane dipole components of the molecules are parallel to each other. This is the same order that we assumed for the molecules in the domains of our theoretical model in Sec. III A. The origin of the contrast in the SH images of the DCANP films is also very similar to our theoretical example. In both cases, the local features (dendrites or domains) exhibit different azimuthal orientations θ of their dipoles with respect to the laboratory frame. Thus they appear with different brightness in an image and can easily be distinguished from each other. The irregular shapes of the local features in the DCANP films will be no problem for the quantitative data evaluation.

A. Homodyne imaging with different phases ϕ_{ref} of the reference signal

Figure 4(a) shows an SH image of a DCANP monolayer on a fused silica substrate. The micrograph was taken in the

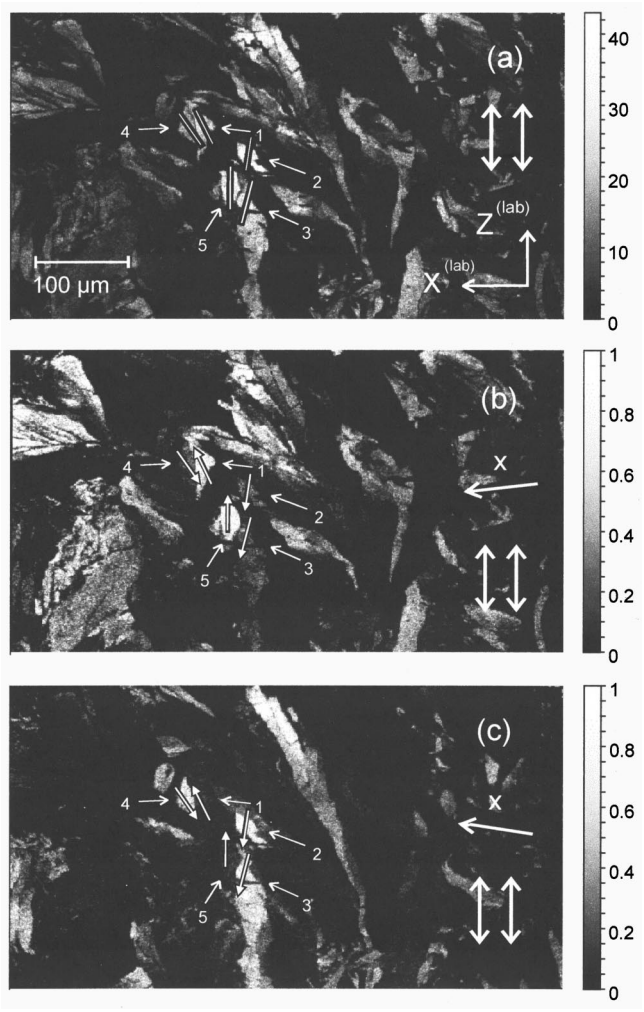

FIG. 4. Second-harmonic images of a DCANP monolayer. (a) Intensity contrast [geometry of Fig. 1(a)]. The gray code is a quantitative measure of the effective second-order optical susceptibility d_{eff} of the film in pm/V. The double-headed arrows represent the orientation of the polarizers. Laboratory coordinates $(X^{(\text{lab})},Z^{(\text{lab})})$ are also shown. The axial orientation of five local features (1–5), calculated from the contrast in the image, is additionally indicated. (b) and (c) Homodyne experiments [geometry of Fig. 1(b)] with different polar orientations of the reference sample (x axis). The gray code in the homodyne images gives the total intensity $I_{\text{tot}}^{(2\omega)}$ in arbitrary units. From the contrast in these images, the absolute orientation of the local features is obtained.

intensity contrast mode of the microscope [geometry of Fig. 1(a)]. The film was observed between parallel polarizers whose orientation is indicated with double-headed arrows in Fig. 4(a). Laboratory coordinates are also shown. The gray code is a quantitative measure of the monolayer's effective susceptibility given in pm/V. Figures 4(b) and 4(c) show the same section of the film in the homodyne experiment [geometry of Fig. 1(b)]. A quartz reference (waveplate) was introduced into the fundamental beam path below the monolayer. The azimuthal orientation of the crystal's x axis is indicated with arrows at the right side of the images. In Fig. 4(b), this polar axis exhibits a projection onto the $-Z^{(\text{lab})}$ axis. In Fig. 4(c), it has a projection onto the $+Z^{(\text{lab})}$ axis. The gray code in Figs. 4(b) and 4(c) gives the intensity of the interference signal in arbitrary units.

The brightness of the local features observed in the intensity contrast image [Fig. 4(a)] depends on the orientation of the local polar Z axis relative to the polarizers according to Eqs. (3) and (4). The validity of Eq. (4) has recently been verified quantitatively for DCANP films at a water surface.[18,19] We verified that the monolayers at a fused silica substrate, investigated here, exhibit the same order. To this end, we turned the polarizers of the intensity contrast microscope synchronously and measured the SH intensities from a large number of local features in different monolayers as a function of the polarizer orientation. The data could be well fitted with Eq. (4). Applying Eq. (4) to the image of Fig. 4(a), we can now calculate the orientations of the local features from the SH intensities with the uncertainty of 180° (axial orientation). For five local objects which are numbered from 1 to 5, the axial orientation is indicated in Fig. 4(a).

The homodyne images of Figs. 4(b) and 4(c) show the same texture as Fig. 4(a) because they were taken from the same area but the contrast is different. The features marked with 1 and 5 exhibit constructive interference in the homodyne experiment of Fig. 4(b) and destructive interference in Fig. 4(c). The features marked with 2, 3, and 4 exhibit the opposite phenomena. Since the polarizer orientation in Fig. 4 corresponds with the $Z^{(\text{lab})}$ axis, all the local objects which radiate an SH signal must have a projection of their Z axis either in the direction of the $+Z^{(\text{lab})}$ axis or in the direction of the $-Z^{(\text{lab})}$ axis. As a first trial, we may assume that the objects which exhibit constructive interference in Fig. 4(b) belong to the former category and all the others to the latter one. The corresponding arrows are given in Figs. 4(b) and 4(c) for the examples of the features 1–5. The attribution of a single-valued orientation to all the local features will facilitate the following quantitative data evaluation. When the phases ϕ_{sam} will be determined we will see if the polar orientation of the local Z axes is as assumed or opposite.

From the Eqs. (4) and (5), we can calculate the SH intensity of the local features in a homodyne experiment. For simplicity, we define a constant A, which stands for all quantities in Eq. (4) that are independent of the orientation θ of a local feature. With $\Psi_p=0°$ in the images of Fig. 4, we can then rewrite Eq. (4) as $I_{\text{sam}}^{(2\omega)}=A\cos^6\theta$. Additionally, we define $B=I_{\text{ref}}^{(2\omega)}$ and $C=2\sqrt{AB}\cos\phi$. We then obtain

$$I_{\text{tot}}^{(2\omega)}=A\cos^6\theta+B+C\cos^3\theta. \tag{9}$$

For the phase ϕ in the quantity C, we have to consider a shift by 180° if we compare the homodyne signals of a local object in Figs. 4(b) and 4(c) [polar axis of the reference with a projection onto the $-Z^{(\text{lab})}$ axis in Fig. 4(b) and a projection onto the $+Z^{(\text{lab})}$ axis in Fig. 4(c)]. If we attribute Eq. (9) to Fig. 4(b), we thus have to describe Fig. 4(c) with the corresponding equation

$$I_{\text{tot}}^{(2\omega)}=A\cos^6\theta+B-C\cos^3\theta. \tag{10}$$

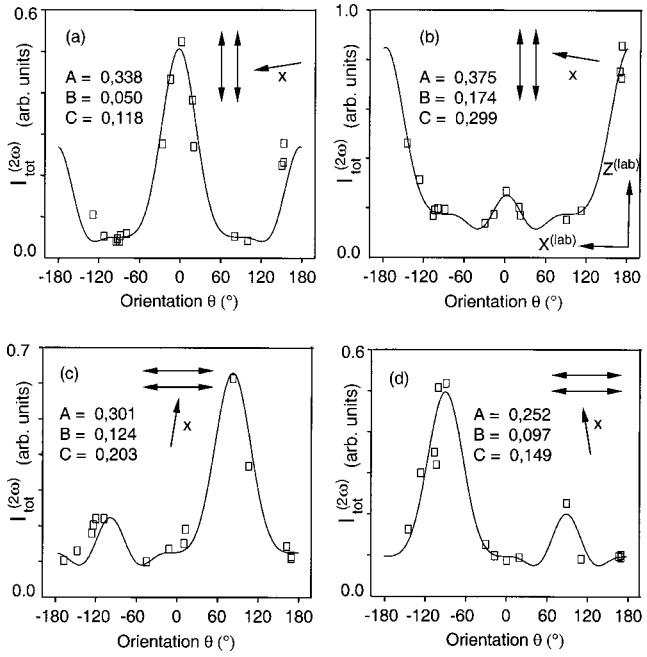

FIG. 5. Measured intensities $I_{\mathrm{tot}}^{(2\omega)}$ (in arbitray units) for various local features as a function of their azimuthal orientation θ in a series of homodyne images. In this series, the experimental geometry was modified as indicated with the orientation of the polarizers (double-headed arrows), the orientation of the quartz reference (x axis), and with laboratory coordinates ($X^{(\mathrm{lab})}$,$Z^{(\mathrm{lab})}$). The lines are a fit of Eqs. (9), (10), (12), and (13) to the data in (a)–(d), respectively. The results of the fits (A, B, C) are also given.

The intensities $I_{\mathrm{tot}}^{(2\omega)}$ for various local features can be determined in a homodyne experiment. The absolute orientations θ of the local features are not known so far but for a plot of $I_{\mathrm{tot}}^{(2\omega)}$ as a function of θ we can apply the convention on the sign of the dipoles introduced above. In this way, the data points of Figs. 5(a) and 5(b) were obtained from the images of Figs. 4(b) and 4(c), respectively. Since the symmetry and order of the local features are identical, we can assume that the phase ϕ is also identical for the objects in an image. Thus we can fit the data in Figs. 5(a) and 5(b) with the corresponding Eqs. (9) and (10), respectively. From the fit parameters A, B, and C, we can determine ϕ according to

$$\cos\phi = \frac{C}{2\sqrt{AB}}. \tag{11}$$

Since the dendrites in Fig. 4 which are oriented unfavorably with respect to the polarizers ($\theta \approx 90°$) do not generate a sufficiently strong SH signal, we took two additional homodyne images with the polarizers parallel to the $X^{(\mathrm{lab})}$ axis ($\Psi_p = 90°$). In one experiment, the polar axis of the reference exhibited a projection onto the $-X^{(\mathrm{lab})}$ axis, in the other one a projection onto the $+X^{(\mathrm{lab})}$ axis. The data are given in Figs. 5(c) and 5(d) together with a fit of the corresponding equations

$$I_{\mathrm{tot}}^{(2\omega)} = A\sin^6\theta + B + C\sin^3\theta \tag{12}$$

and

$$I_{\mathrm{tot}}^{(2\omega)} = A\sin^6\theta + B - C\sin^3\theta, \tag{13}$$

respectively. In Fig. 5, the results for the fit parameters are given in arbitrary units.

Using Eq. (11), we can now calculate the phase ϕ for the four images. Since ϕ, however, is the argument of a cosine function, we obtain two possible values $\phi^{(1)}$ and $\phi^{(2)}$. The results obtained from the data in Fig. 5 and from a second series of images, measured with another DCANP monolayer, are $\phi^{(1)} = 62° \pm 9°$ and $\phi^{(2)} = 298° \pm 9°$. From these quantities, two possible values for the sample phase, $\phi_{\mathrm{sam}}^{(1)}$ and $\phi_{\mathrm{sam}}^{(2)}$, can be calculated by applying Eq. (6). The phase of the reference in Eq. (6) can be obtained from the thickness and refractive indices of the waveplate (see Sec. IV) by applying Eq. (8). The result is $\phi_{\mathrm{ref}} = -3° \pm 3°$. The phase shift ϕ_Δ in Eq. (6) is the sum of two contributions ϕ_{air} and $\phi_{\delta\mathrm{sub}}$, which originate from the air between the two SH light sources in the imaging experiment and from the substrate of the monolayer, respectively. The contribution from the substrate can be calculated from its thickness and its refractive indices (see Sec. IV) to be $\phi_{\delta\mathrm{sub}} = -254° \pm 7°$. With a distance of 36.55 cm between the top surface of the reference and the bottom side of the monolayer's substrate and with $L_{360} = 12.66$ cm for the air measured directly after having taken the monolayer images, we obtain $\phi_{\mathrm{air}} = -319° \pm 3°$. Thus $\phi_\Delta = -213° \pm 8°$. Using Eq. (6), we finally find the results $\phi_{\mathrm{sam}}^{(1)} = -150° \pm 10°$ and $\phi_{\mathrm{sam}}^{(2)} = 80° \pm 10°$. The latter quantity is the physically significant phase. It agrees with the expected result of $\phi_{\mathrm{sam}} \approx 90°$. Thus the sign of the local features' polar orientation is as we assumed above [Figs. 4(b) and 4(c)]. If we had assumed the opposite orientation for all the local features, our result would be $\phi_{\mathrm{sam}}^{(2)} \approx -90°$.

B. Homodyne imaging by using the gas cell in order to alter the phases ϕ_Δ

Applying the experiment of Fig. 1(c), a series of homodyne images was taken from a section of a monolayer. In this series, the gas pressure was altered in order to change the phase ϕ_Δ [Eq. (6)]. The orientation of the polarizers and the quartz waveplate was identical to the geometry of Fig. 4(b). Figure 6 shows the intensities $I_{\mathrm{tot}}^{(2\omega)}$ for two different local features, called 1 and 2, in the imaged surface section as a function of the gas pressure. After the micrographs had been obtained we replaced the monolayer sample by a second quartz reference. A series of images from its top surface was then taken. In this series, the gas pressure was altered as in the monolayer study. The homodyne intensity in the reference experiment as a function of the pressure is also given in Fig. 6 for a section of the imaged crystal surface. The location of this section corresponds to the position of feature 2 in the homodyne image of the monolayer.

We determined also individual reference curves for all the local features investigated in the monolayer sample. Phase shifts of a few degrees between the reference curves for the different lateral positions were observed. This is probably due to slight lateral variations in the thickness of the quartz

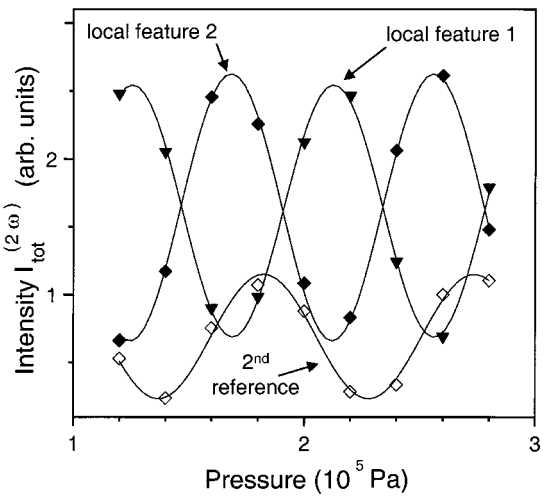

FIG. 6. Measured intensities $I_{\mathrm{tot}}^{(2\omega)}$ as a function of the pressure in gas cell. The results for two local features in an image, called 1 and 2, are shown. The reference data for feature 2 are also given. The curves are fits of Eq. (5) together with Eqs. (14) and (15) to the monolayer and reference data, respectively.

platelets. Below, we compensate for these phase variations by comparing the data of any local feature with its individual reference curve.

In order to fit the data in Fig. 6 we have to consider that the phase ϕ_Δ in the experiments is composed of various contributions. In the monolayer images, $\phi_\Delta = \phi_p + \phi_{\delta\mathrm{sub}} + \phi_{\mathrm{win,air}}$ where ϕ_p is the variable phase which is proportional to the absolute pressure in the nitrogen cell, $\phi_{\delta\mathrm{sub}}$ is the phase shift which originates from the substrate of the monolayer, and $\phi_{\mathrm{win,air}}$ is the phase shift due to the windows of the pressure cell and air in the space between the two SH light sources. Substituting ϕ_Δ in Eq. (6) by these contributions, we obtain

$$\phi = \phi_{\mathrm{sam}} - \phi_{\mathrm{ref}} - \phi_p - \phi_{\delta\mathrm{sub}} - \phi_{\mathrm{win,air}}. \tag{14}$$

The analogous formula for the homodyne experiment with the second reference is

$$\phi_{\mathrm{ref,ref*}} = \phi_{\mathrm{ref*}} - \phi_{\mathrm{ref}} - \phi_p - \phi_{\delta\mathrm{ref*}} - \phi_{\mathrm{win,air}}, \tag{15}$$

where $\phi_{\mathrm{ref,ref*}}$ is the phase difference of the SH signals from the two reference samples and $\phi_{\mathrm{ref*}}$ is the phase of the signal from the second reference. The quantity $\phi_{\delta\mathrm{ref*}}$ is the phase shift that the SH light from the quartz waveplate suffers when it propagates through the second reference.

The curves in Fig. 6 are fits of Eq. (5) together with Eqs. (14) and (15) to the monolayer and the reference data, respectively. A comparison of the curves for the two local features in Fig. 6 shows directly that their relative phase is $\sim 180°$. The absolute phases ϕ_{sam} of the local objects cannot be obtained from these curves alone because the quantity $\phi_{\mathrm{win,air}}$ [Eq. (14)] is not known in our study. The reference curve [Eq. (15)], however, provides additional information. Using Eqs. (14) and (15), we can calculate the absolute local phase to be

$$\phi_{\mathrm{sam}} = \phi - \phi_{\mathrm{ref,ref*}} + \phi_{\mathrm{ref*}} - \phi_{\delta\mathrm{ref*}} + \phi_{\delta\mathrm{sub}}. \tag{16}$$

The relative phase $\phi - \phi_{\mathrm{ref,ref*}}$ for a local feature is directly accessible from a comparison of its interference curve with the corresponding reference curve. From these data, ϕ_{sam} can then be calculated because the other quantities in Eq. (16) are known. With the data given in Sec. IV, we obtain $\phi_{\mathrm{ref*}} = 49° \pm 3°$ [Eq. (8)], $\phi_{\delta\mathrm{ref*}} = -82° \pm 4°$, and $\phi_{\delta\mathrm{sub}} = -254° \pm 7°$.

The relative phase of $\sim 180°$ observed in Fig. 6 for two local features means that one of them exhibits a projection of its dipole onto the $+Z^{(\mathrm{lab})}$ axis of the laboratory frame; the other one has a projection onto the $-Z^{(\mathrm{lab})}$ axis. For all the other local features, we expect that they can be divided into two groups. The objects of one group should exhibit the same absolute phase ϕ_{sam} as the object 1 in Fig. 6. The absolute phases of the other local features should be shifted by 180°. In total, we investigated 18 different local objects in the monolayer. Actually, we found two values for their phases with respect to the reference phase, $(\phi - \phi_{\mathrm{ref,ref*}})^{(1)} = -132° \pm 10°$ for the population which includes feature 1, and $(\phi - \phi_{\mathrm{ref,ref*}})^{(2)} = 46° \pm 10°$ for the population which includes feature 2. The result for the absolute phases is $\phi_{\mathrm{sam}}^{(1)} = 110° \pm 10°$ and $\phi_{\mathrm{sam}}^{(2)} = -80° \pm 10°$, which agrees with the expected phase of $\phi_{\mathrm{sam}} \approx 90°$. This result means that the features of the former population (feature 1) exhibit a projection of their polar axes onto the $-Z^{(\mathrm{lab})}$ axis of the laboratory coordinates on which the polar axes of the reference crystals have also a projection. The latter population (feature 2) exhibits a projection onto the $+Z^{(\mathrm{lab})}$ axis.

VI. CONCLUSION

The two techniques used in this study allowed us to determine the absolute phase of any local feature which was clearly resolved in the images. From the data, the two-dimensional distribution of the absolute polar orientation at an interface can be determined with far-field optical resolution. The first method is particularly simple. It, however, provides the phases with a mathematical ambiguity. Using additional spectroscopic information in our off-resonance study of DCANP monolayers we could easily find out which of the two possible results is the physically significant one. In other experiments which are carried out near resonance it may, however, often be difficult to decide which of the two calculated phases is the physically correct result. In such cases, the second method which takes advantage of the additional phase shifter should be used. This technique provides the absolute local phases unambiguously.

It should additionally be emphasized that our example of a monolayer where all the local objects had the same molecular order (point group) is not an exotic case. All polycrystalline surfaces, for example, exhibit similar phenomena. In such examples, a few images taken with different orientations of the polarizers and the reference samples are sufficient for the determination of the local phases. The two techniques, however, are not restricted to such simple cases. At other surfaces, different local objects may exhibit a different symmetry and order. Then, a larger number of images must be taken in a series of modified geometries in order to obtain a sufficient number of data for any individual local object.

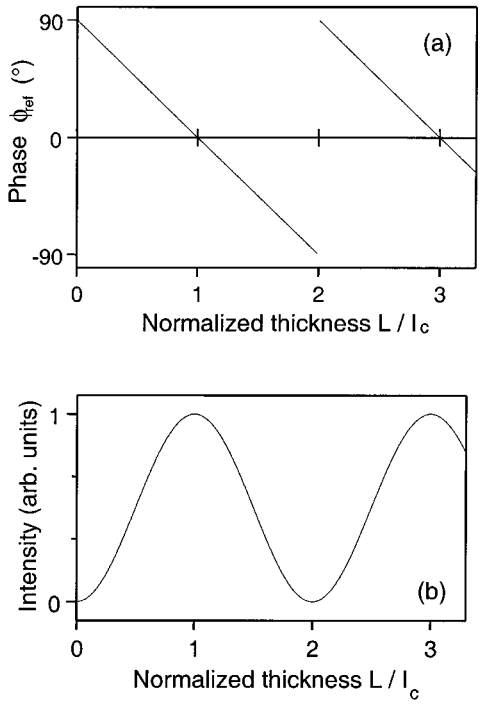

FIG. 7. (a) Calculated phase and (b) second-harmonic intensity of the reference crystal as a function of the normalized thickness L/l_c.

In conclusion, we have shown that the absolute phases and the sign of the polar molecular orientation at an interface can be measured with two-dimensional far-field optical resolution. Knowledge of the polar orientation field is important, for example, for the development of new polar bulk materials which are grown from surfaces. The phases of the susceptibilities are also required for the molecular interpretation if tensor elements with different phases contribute to the nonlinear signal.

ACKNOWLEDGMENTS

We appreciate helpful discussions on the crystal structure and the properties of α-quartz with Th. Krol (Institute for Materials Physics, Münster), J. Löns, D. Bosbach (Institute for Mineralogy, Münster), H. Hellwig (Geophysical Laboratory, Carnegie Institution of Washington, D.C.), and J. Schreuer (Laboratory of Crystallography, Swiss Federal Institute of Technology, Zürich). Also, financial support from the Volkswagen Foundation and the Federal Ministry for School, Advanced Education, Science and Research of Northrhine-Westfalia is gratefully acknowledged.

APPENDIX

Here we calculate the phase ϕ_{ref} of the SH wave generated in a reference crystal. The fundamental light in our experiments propagates in the $+y$ direction of the crystal coordinate system [see Fig. 1(b)]. In the reference sample, an SH signal is generated which propagates in forward direction. The entrance plane for the laser light may be located at $y=0$. The exit plane lies then at $y=L$. The interaction of the fundamental and SH waves in the nonlinear optical medium is described with a system of coupled-amplitude equations.[48] For plane waves under the nondepleted pump approximation in a lossless medium, the evolution of the SH amplitude $E^{(2\omega)}$ is given by

$$\frac{dE^{(2\omega)}}{dy}=\frac{32\pi i\omega^2}{k^{(2\omega)}c^2}d_{\mathrm{eff}}(E^{(\omega)})^2e^{i\Delta ky}, \tag{A1}$$

with $E^{(\omega)}$ the fundamental amplitude,

$$\Delta k=2k^{(\omega)}-k^{(2\omega)} \tag{A2}$$

the momentum mismatch, $k^{(\omega)}$ the wave vector at the laser frequency, and $k^{(2\omega)}$ the wave vector at the SH frequency. By integrating Eq. (A1) from $y=0$ to $y=L$ we can calculate the SH field at the exit face of the crystal to be

$$E^{(2\omega)}=\frac{32\pi i\omega^2}{k^{(2\omega)}c^2}d_{\mathrm{eff}}(E^{(\omega)})^2\int_0^L e^{i\Delta ky}$$

$$=\frac{32\pi\omega^2}{k^{(2\omega)}c^2}d_{\mathrm{eff}}(E^{(\omega)})^2\frac{e^{i\Delta kL}-1}{\Delta k}. \tag{A3}$$

The phase of $E^{(2\omega)}$ depends on the factor $e^{i\Delta kL}-1$. Its imaginary part is $\mathrm{Im}(e^{i\Delta kL}-1)=\sin\Delta kL$. Its real part is $\mathrm{Re}(e^{i\Delta kL}-1)=\cos\Delta kL-1$. The phase ϕ_{ref} of $E^{(2\omega)}$ is thus

$$\phi_{\mathrm{ref}}=\arctan\left(\frac{\sin(\Delta kL)}{\cos(\Delta kL)-1}\right). \tag{A4}$$

This expression can be written as

$$\phi_{\mathrm{ref}}=\arctan\left(\frac{\sin\left(\frac{4\pi(n^{(\omega)}-n^{(2\omega)})L}{\lambda_0}\right)}{\cos\left(\frac{4\pi(n^{(\omega)}-n^{(2\omega)})L}{\lambda_0}\right)-1}\right)$$

$$=\arctan\left(\frac{\sin\left(-\pi\frac{L}{l_c}\right)}{\cos\left(-\pi\frac{L}{l_c}\right)-1}\right), \tag{A5}$$

with $l_c=\lambda_0/4|n^{(\omega)}-n^{(2\omega)}|$ the coherence length of the nonlinear interaction process. The arguments of the sine and cosine functions in Eqs. (A4) and (A5) are negative for a material with normal dispersion such as quartz in the spectral region of our experiments. In Fig. 7(a), ϕ_{ref} is plotted as a function of the normalized thickness L/l_c of a noncentrosymmetric material. For comparison, the well-known dependence of the SH intensity on L/l_c is given in Fig. 7(b). The typical spatial oscillations of the intensity in the case of phase mismatch ($\Delta k\neq 0$) can be seen. Under this condition,

ϕ_{ref} exhibits also spatial variations. If L is an odd multiple of l_c, the phase of the reference with respect to the fundamental light is $\phi_{\mathrm{ref}}=0°$. At such positions, no energy is transferred between the fundamental and SH waves. At positions which correspond to even multiples of l_c, the phase changes between $\phi_{\mathrm{ref}}=-90°$ (energy transfer from the harmonic to the fundamental wave) and $\phi_{\mathrm{ref}}=90°$ (energy transfer to the harmonic wave).

*Corresponding author. Present address: Institute for Nuclear Waste Management, Karlsruhe Research Center, P.O. Box 3640, D-76021 Karlsruhe, Germany. Electronic address: florshg@ine.fzk.de

†Present address: Institute of Applied Physics and Center for Microstructure Research, University of Hamburg, Jungiusstraße 11, D-20355 Hamburg, Germany.

[1] Y. R. Shen, Nature (London) **337**, 519 (1989).
[2] V. Vogel and Y. R. Shen, Annu. Rev. Mater. Sci. **21**, 515 (1991).
[3] Y. R. Shen, Surf. Sci. **299/300**, 551 (1994).
[4] R. M. Corn and D. A. Higgins, Chem. Rev. **94**, 107 (1994).
[5] C. D. Bain, J. Chem. Soc., Faraday Trans. **91**, 1281 (1995).
[6] K. B. Eisenthal, Chem. Rev. **96**, 1343 (1996).
[7] D. E. Gragson and G. L. Richmond, J. Phys. Chem. B **102**, 3847 (1998).
[8] J. F. McGilp, in *Progress in Surface Science*, edited by S. G. Davison and P. G. Davison (Elsevier Science, Oxford, 1995), pp. 1–105.
[9] G. Lüpke, Surf. Sci. Rep. **35**, 75 (1999).
[10] G. T. Boyd, Y. R. Shen, and T. W. Hänsch, Opt. Lett. **11**, 97 (1986).
[11] K. A. Schultz and E. G. Seebauer, J. Chem. Phys. **97**, 6958 (1992).
[12] M. Flörsheimer, H. Looser, M. Küpfer, and P. Günter, in *Proceedings of the Sixth International Conference on Organized Molecular Films*, Trois-Rivières, Canada, 1993 [Thin Solid Films **244**, 1001 (1994)].
[13] L. Smilowitz, Q. X. Jia, X. Yang, D. Q. Li, D. McBranch, S. J. Buelow, and J. M. Robinson, J. Appl. Phys. **81**, 2051 (1997).
[14] M. Cernusca, M. Hofer, and G. A. Reider, J. Opt. Soc. Am. B **15**, 2476 (1998).
[15] N. Kato, K. Saito, and Y. Uesu, Thin Solid Films **338**, 5 (1999).
[16] Th. Rasing, Appl. Phys. B: Lasers Opt. **68**, 477 (1999).
[17] Y. Sonoda, G. Mizutani, H. Sano, S. Ushioda, T. Sekiya, and S. Kurita, Jpn. J. Appl. Phys., Part 2 **39**, L253 (2000).
[18] M. Flörsheimer, M. Bösch, Ch. Brillert, M. Wierschem, and H. Fuchs, Supramol. Sci. **4**, 255 (1997).
[19] M. Flörsheimer, H. Salmen, M. Bösch, Ch. Brillert, and H. Fuchs, Adv. Mater. **9**, 1056 (1997).
[20] M. Flörsheimer, Ch. Brillert, and H. Fuchs, Langmuir **15**, 5437 (1999).
[21] M. Buck, Appl. Phys. A: Solids Surf. **55**, 395 (1993).
[22] R. Reiter, H. Motschmann, H. Orendi, A. Nemetz, and W. Knoll, Langmuir **8**, 1784 (1992).
[23] S. Hénon and J. Meunier, Rev. Sci. Instrum. **62**, 936 (1991).
[24] D. Hönig and D. Möbius, Thin Solid Films **210/211**, 64 (1992).
[25] H. H. Rotermund, G. Haas, R. U. Franz, R. M. Tromp, and G. Ertl, Science **270**, 608 (1995).
[26] K. Kemnitz, K. Bhattacharyya, J. M. Hicks, G. R. Pinto, K. B. Eisenthal, and T. F. Heinz, Chem. Phys. Lett. **131**, 285 (1986).
[27] R. Superfine, J. Y. Huang, and Y. R. Shen, Phys. Rev. Lett. **66**, 1066 (1991).
[28] Q. Du, R. Superfine, E. Freysz, and Y. R. Shen, Phys. Rev. Lett. **70**, 2313 (1993).
[29] O. Sato, R. Baba, K. Hashimoto, and A. Fujishima, Jpn. J. Appl. Phys., Part 1 **32**, 1201 (1993).
[30] M. Buck, F. Eisert, M. Grunze, and F. Träger, Appl. Phys. A: Mater. Sci. Process. **60**, 1 (1995).
[31] R. Stolle, G. Marowsky, E. Schwarzberg, and G. Berkovic, Appl. Phys. B: Lasers Opt. **63**, 491 (1996).
[32] U. Höfer, Appl. Phys. A: Mater. Sci. Process. **63**, 533 (1996).
[33] K. Kajikawa, L.-M. Wang, T. Isoshima, T. Wada, W. Knoll, H. Sasabe, S. Okada, and H. Nakanishi, Thin Solid Films **284–285**, 612 (1996).
[34] R. Schliesing, G. Eichhorn, X. Jiang, and H. Zacharias, Surf. Sci. **387**, 279 (1997).
[35] F. Eisert, O. Dannenberger, and M. Buck, Phys. Rev. B **58**, 10 860 (1998).
[36] X. Zhuang, P. B. Miranda, D. Kim, and Y. R. Shen, Phys. Rev. B **59**, 12 632 (1999).
[37] J. I. Dadap, J. Shan, A. S. Weling, J. A. Misewich, and T. F. Heinz, Appl. Phys. B: Lasers Opt. **68**, 333 (1999).
[38] M. Fiebig, D. Fröhlich, St. Leute, and R. V. Pisarev, Appl. Phys. B: Lasers Opt. **66**, 265 (1998).
[39] M. Flörsheimer, Phys. Status Solidi A **173**, 15 (1999).
[40] M. Flörsheimer, M.-Th. Bootsmann, and H. Fuchs, Adv. Mater. **12**, 1918 (2000).
[41] V. Mizrahi and J. E. Sipe, J. Opt. Soc. Am. B **5**, 660 (1988).
[42] *Elastische, piezoelektrische, piezooptische Konstanten und nichtlineare dielektrische Suszeptibilitäten von Kristallen*, edited by K.-H. Hellwege and A. M. Hellwege, Landolt-Börnstein, New Series, Vol. III/11 (Springer, Berlin, 1979). For the susceptibility of quartz we used the arithmetic average $d_{xxx}=0.4$ pm/V of the values reported there.
[43] Steeg & Reuter (personal communication).
[44] J. Jerphagnon and S. K. Kurtz, J. Appl. Phys. **41**, 1667 (1970).
[45] Hellma (personal communication).
[46] D. E. Lynch, U. Geissler, I. R. Peterson, M. Flörsheimer, R. Terbrack, L. F. Chi, H. Fuchs, N. J. Calos, B. Wood, C. H. L. Kennard, and G. J. Langley, J. Chem. Soc., Perkin Trans. 2 **1997**, 827 (1997).
[47] M. Flörsheimer, M. Bösch, Ch. Brillert, and H. Fuchs, Adv. Mater. **9**, 1061 (1997).
[48] R. W. Boyd, *Nonlinear Optics* (Academic, San Diego, 1992), Chap. 2.2.